Hyperfine Sublevel Correlation Spectroscopy Studies of Iron-Sulfur Cluster in Rieske Protein from Green Sulfur Bacterium *Chlorobaculum tepidum*

Hiroki Nagashima[1], Hiraku Kishimoto[2], Risa Mutoh[3], Naotaka Terashima[1], Hirozo Oh-oka[2], Genji Kurisu[2,3] and Hiroyuki Mino[1]*

[1]Division of Material Science, Graduate School of Science, Nagoya University, Furo-cho, Chikusa-ku, Nagoya, Aichi, 464-8602, Japan

[2]Department of Biological Sciences, Graduate School of Science, Osaka University, Toyonaka, Osaka, 560-0043, Japan

[3]Institute for Protein Research, Osaka University, Suita, Osaka, 565-0871, Japan

Supporting Information Placeholder

ABSTRACT: The magnetic properties of the Rieske protein, purified from *Chlorobaculum tepidum* were investigated using electron paramagnetic resonance and hyperfine sublevel correlation spectroscopy (HYSCORE). The g-values of the Fe_2S_2 center were g_x = 1.81, g_y = 1.90, and g_z = 2.03. Four classes of nitrogen signals were obtained by HYSCORE. Nitrogens 1 and 2 had relatively strong magnetic hyperfine couplings and were assigned as the nitrogen directly ligated to Fe. Nitrogens 3 and 4 had relatively weak magnetic hyperfine couplings and were assigned as the other nitrogen of the histidine ligands and peptide nitrogen connected to the sulfur atom via hydrogen bonding, respectively. The anisotropy of the nitrogen 3 reflects the different spin density distributions on the histidine ligands, which influences the electron transfer to the quinone.

Introduction

Cytochrome (cyt) *bc* complexes are crucial energy-transducing machineries in respiratory and photosynthetic electron transport chains. They conduct characteristic quinol oxidation reactions that couple electron transport with proton translocation across membranes, resulting in the production of an electrochemical proton gradient or proton motive force essential for ATP synthesis. These reactions are now well understood as the Q-cycle mechanism.[1]

Recently, genome-wide analyses have shown that the minimal functional and mechanistic unit of the Q-cycle mechanism consists of Rieske iron-sulfur protein (ISP) and cyt *b*.[2] This catalytic core evolved into various complexes by incorporating structurally unrelated proteins. For example, cyt bc_1 and b_6f complexes have incorporated cyt c_1 and *f*, respectively, as secondary electron carriers. In phototrophic green sulfur bacteria (or Chlorobiaceae), the *petC* gene coding for *c*-type cyt is absent in the transcriptional unit of the *petCB* genes for Rieske ISP and cyt *b*, indicating that its cyt *bc* complex would be of the Rieske/cyt *b* type.[3, 4] Moreover, phylogenetic analyses have also suggested that cyt *b* in green sulfur bacteria splits into cyt b_6 and subunit IV before its divergence to cyt b_6-type complexes in heliobacteria (cyt b_6cc) and cyanobacteria (cyt b_6f).[5]

The Rieske/cyt *b* unit utilizes two categorized pool quinones, that is, low and high potential quinones, in order to produce the proton motive force across membranes.[6] The low potential menaquinone (MK, E_m = ~ -70 mV) is considered to be the ancestral type of quinone. Vast ranges of prokaryotes including green sulfur bacteria and heliobacteria, which inhabit mostly anaerobic environments, oxidize menaquinol at the Q_o site to induce the bifurcated electron transfer reactions. On the other hand,

almost all proteobacteria (and mitochondria) including phototrophic purple bacteria, cyanobacteria (and chloroplasts), and hyperthermophilic aerobic archaebacteria, which adapted to the modern oxygenic atmosphere, possess the high potential quinones ($E_m = \sim 100$ mV): ubiquinone (proteobacteria), plastoquinone (PQ) (cyanobacteria), and caldariellaquinone (Sulfolobus spp.). From the viewpoint of evolutionary processes in chemiosmotic energy-converting systems, it would have been critical for MK-type cyt bc complexes to commence utilization of higher potential quinones in the transition from anaerobic to aerobic conditions induced by the action of oxygenic photosynthesis.[2] Without any upshift of the redox potentials of cofactors in this enzyme, especially those of the Rieske cluster, higher potential quinones were very poor electron donors for the retrieval of electrochemical energy. In fact, the Rieske/cytochrome b complex in green sulfur bacteria is positioned just before the divergence to a PQ-type cyt b_6f complex in the phylogenetic tree.[2] The redox potential of its Rieske ISP ($E_m = \sim 160$ mV) is expected to up-shift in accordance with the difference in potentials between MK and PQ.

The way in which redox potentials of various Rieske clusters could be tuned so as to be energetically favorable in variable energy conversion systems has been a subject of discussion for many years. There are two types of iron-sulfur clusters: the high potential type with E_m between +105 and +490 mV, and the low potential type with E_m between -155 and -50 mV.[7-9] Iron sulfur cluster [2Fe-2S] consists of two iron atoms bridged by two sulfur atoms. As two histidine and two cysteine residues are ligated to two Fe atoms, the backbone structures of Fe_2S_2 are common among all the species. Multiple factors surrounding the [2Fe-2S] cluster would thus be involved in the optimization of the redox potential suitable for its reaction partner.

The factors that determine the midpoint potential of the Rieske cluster, [2Fe-2S] have been reported. Density functional theory (DFT) calculations suggested that the negatively charged amino acid residues near the cluster modulate the midpoint potential[6, 10-13]. The H-bond network has also been recognized as an important factor in the determination of the redox potential[12-15]. Fig. 1 shows the amino acid sequence alignments of Rieske protein from photosynthetic organisms such as spinach, *Rhodobacter sphaeroides*, and *Chlorobaculum. tepidum*. Four

amino acid residues, ligated to the iron-sulfur cluster[16], are well conserved. Fig. 2A shows the crystal structures of Rieske protein from spinach[16] and Fig. 2B shows the comparison between the structures of spinach and purple bacteria (*R. sphaeroides*)[11]. Their structures surrounding the iron-sulfur clusters are very similar. In spinach, two cysteine residues, Cys107 and Cys125, are ligated to a Fe ion, denoted as Fe_1, and two histidine residues, H109 and H128, are ligated to another Fe ion, denoted as Fe_2. The peptide nitrogen of Leu110 (132) and oxygen of Ser130 (154) residue in spinach (*R.sphaeroides*) are hydrogen-bonded to the bridging sulfur atom. The Tyr132 (156) residue also has a hydrogen bond to Cys107 (149). These hydrogen bonds have been found to affect the midpoint potential of the Rieske cluster. Site-directed mutagenesis studies revealed that the substitutions of Ala and Phe for Ser130(154) and Tyr132(156), respectively, induced the drastic decrease of midpoint potentials and rates of quinone oxidation[12, 13, 15]. The removal of the hydrogen bond from the cluster would possibly modify the geometry and electronic structure of the iron-sulfur center, although their X-ray crystal structures are unknown. In the case of the Rieske protein in *C. tepidum*, Ser130(154) in spinach (*R. sphaeroides*) is replaced by alanine and its relatively lower midpoint potential is reasonable, because it has one less H-bond than in spinach and *R. sphaeroides*. However, more spectroscopic data of the Rieske protein in *C. tepidum* are needed to understand the physicochemical properties of its iron-sulfur cluster fully.

Electron paramagnetic resonance (EPR) is a powerful tool for investigating the electronic and magnetic structure of paramagnetic species. The reduced [2Fe-2S] cluster has a ground state of $S = 1/2$, and EPR signals are detected around the $g = 2$ region with rhombic symmetry. Electron spin echo envelope modulation (ESEEM) is one of the advanced EPR techniques that can selectively detect nuclear magnetic species (e.g. ^{14}N, ^{15}N, ^{1}H, ^{2}H) surrounding a paramagnetic center. Four-pulsed ESEEM spectroscopy, called hyperfine sublevel correlation spectroscopy (HYSCORE) can resolve several peaks in two dimensions, thus making spectra interpretation easy[17]. HYSCORE facilitates an understanding of the electronic structure, direct ligands, and hydrogen bonding in amino acids.

In this study, we investigated the electronic structure of Rieske protein from a green-sulfur bacterium, *C. tepidum*, by ESEEM and $^{14}N/^{15}N$-

2

HYSCORE. The EPR data obtained were compared with those from other Rieske proteins.

2. Materials and Methods

2.1 Sample preparations

An N-terminally truncated Rieske protein (PetC), whose gene was cloned into the pET21a vector, was expressed in *Escherichia coli* strain C41(DE3) cells harboring the plasmid pRKISC in an Luria-Bertani (LB) medium for ^{14}N Rieske Protein and M9 minimal medium (containing ^{15}NH$_4$Cl as the sole nitrogen source) for ^{15}N labeled Rieske Protein. The pRKISC contains the *isc* gene cluster involved in the assembly of the Fe-S cluster[18]. A detailed method for the construction of the expression vector of PetC will be described in a future publication (Kishimoto et al., Osaka University). The cells were harvested after cultivation, and applied to an Ni^{2+}-*NTA* affinity column (QIAGEN) equilibrated with 50 mM Tris-HCl of pH=8.0 and 300 mM NaCl, and eluted with 50 mM Tris-HCl of pH=8.0, 300 mM NaCl, and 250 mM imidazole. They were subsequently applied to a HiLoad 26/600 Superdex 75 pg (GE Healthcare) column equilibrated with 20 mM Tris-HCl of pH=7.5 and 50 mM NaCl. The purified samples were frozen in liquid nitrogen until use. The protein concentration was estimated by spectrophotometry at 280 nm. For the EPR measurements, approximately 30 mM sodium dithionite was added to 30 mM Rieske protein with 20 mM Tris-HCl of pH 7.5 and 50 mM NaCl.

2.2 EPR measurements

A Bruker E580 spectrometer was used to measure EPR signals, equipped with a dielectric sapphire resonator (ER 4118X-MD-5). The temperature was controlled using an Oxford gas flow temperature control system CF935 and measurements were performed at 12 K. The pulse sequences of the one-dimensional three-pulse electron spin echo envelope modulation (stimulated ESEEM) and the two-dimensional four-pulse ESEEM (HYSCORE) were $\pi/2$-τ-$\pi/2$-T-$\pi/2$-τ-echo and $\pi/2$-τ-$\pi/2$-T_y-π-T_x-$\pi/2$-τ-echo, respectively. The pulse lengths of the π- and $\pi/2$-pulses were 32 ns and 16 ns, respectively. 4-step phase cycling was employed for the ESEEM and HYSCORE experiments to eliminate unwanted echoes. In the three-pulse ESEEM and HYSCORE experiments, echo intensities (integrated using 92 ns and 40 ns gate width for ESEEM and HYSCORE, respectively) were recorded with varying T for 2048 points

in 4 ns steps and with varying T_x and T_y for 512 points in 16 ns steps, respectively. The time domain ESEEM spectra were converted to the frequency domain by Fourier transformation after subtracting the decay components. No zero-fillings were performed before the two-dimensional Fourier transformation. To eliminate blind spots, multiple τ values were employed in the ESEEM and HYSCORE experiments (see figure captions). ^{14}N-HYSCORE spectra were also measured using another condition where τ was 188, 200, and 220 ns and T_x and T_y were varied over 256 points in 16 ns steps. The final HYSCORE spectra were composed of the sum of HYSCORE spectra measured at different τ, where the spectra were normalized by the exponential fitting of the decay components of the time domain spectra.

2.3 Analysis of ESEEM and HYSCORE spectra

Fig. 3 shows the energy diagram of the ^{14}N and ^{15}N nuclear spin interaction with unpaired electron spin. The nuclear frequencies between each sublevel are detectable using ESEEM and HYSCORE spectroscopy. In the HYSCORE method, peaks are detected two-dimensionally in the frequency domain spectra. The non-diagonal cross peaks show the pair of nuclear frequencies from opposite electron-spin manifolds. Thus, HYSCORE spectra facilitate the assignment of nuclear frequencies and resolves overlapping peaks in the three-pulse ESEEM spectra.

^{14}N ($I = 1$) has three sublevels in each electron-spin manifold and there are three possible transitions (two single quantum (sq) and one double quantum (dq) transition (Fig. 3)). ^{14}N can produce up to 18 cross peaks in the frequency domain of HYSCORE spectra[19]. In contrast, ^{15}N ($I = 1/2$) has only two sublevels in each electron-spin manifold and there is only one nuclear transition in each manifold. Thus, single ^{15}N shows only two peaks in ^{15}N-HYSCORE signals at (ν_{+sq}, ν_{-sq}) and (ν_{-sq}, ν_{+sq}) that can be interpreted without difficulty.

When the hyperfine interaction dominates the ^{14}N nuclear frequencies, the first order expressions are described [17, 20, 21] as:

$$\nu_{1sq\pm} = \frac{A_{1n}}{2} \pm \nu_I + \frac{3Q_n}{2} \qquad (1)$$

$$\nu_{2sq\pm} = \frac{A_{1n}}{2} \pm \nu_I - \frac{3Q_n}{2} \qquad (2)$$

3

$$\nu_{dq\pm} = A_{1n} \pm 2\nu_I \qquad (3)$$

where, ν_I is the Zeeman frequency, A_{1n} is hyperfine coupling, Q_n is quadrupole coupling at arbitrary orientation of the external magnetic field in the selected coordinate system. The second order expressions of the nuclear frequencies are as follows[17, 21]:

$$\nu_{(1,2)sq+}^{(2)} = \frac{A^{(2)} \pm Q^{(2)}}{A_n - 2\nu_I} \qquad (4)$$

$$\nu_{(1,2)sq-}^{(2)} = \frac{A^{(2)} \pm Q^{(2)}}{A_n + 2\nu_I} \qquad (5)$$

$$\nu_{dq\pm}^{(2)} = \frac{A^{(2)}}{\frac{A_n}{2} \pm \nu_I} \qquad (6)$$

where,

$$A^{(2)} = \frac{T_{np}^2 + T_{nq}^2}{4} + K^2(3 + \eta^2) - \frac{3Q_n^2}{4} \qquad (7)$$

$$Q^{(2)} = 3(Q_{np}T_{np} + Q_{nq}T_{nq}) \qquad (8)$$

$$A_n = \frac{2\nu_I(\nu_{dq+} + \nu_{dq-})}{8\nu_I - (\nu_{dq+} - \nu_{dq-})} \qquad (9)$$

where, $K = e^2qQ/4h$ is the quadrupole coupling constant and η is the asymmetry parameter. The matrix T in $A^{(2)}$ and $Q^{(2)}$ is the anisotropic part of the hyperfine interaction. n represents the orientation of the external magnetic field. p and q are two orientations perpendicular to n and each other.[17] The hyperfine and quadrupole parameters reported in this article were obtained using formulas (1)-(3) and (9).

The nuclear frequency of the ^{15}N interacting with an unpaired spin is expressed as:

$$\nu_{\pm} = \left| \frac{A}{2} \pm \nu_I \right| \qquad (10)$$

From this equation, hyperfine constants are determined from observed pairs of peaks. The amplitude of hyperfine interaction and nuclear Zeeman frequencies of ^{15}N is converted to those of ^{14}N using fundamental nuclear properties:

$$\left| \frac{A(^{15}N)}{A(^{14}N)} \right| = \left| \frac{\nu(^{15}N)}{\nu(^{14}N)} \right| = 1.403 \qquad (11)$$

3. Results

3.1 CW-EPR

Fig. 4 shows the continuous wave (CW)-EPR spectra of the Rieske protein from *C. tepidum*. In the oxidized [2Fe-2S] cluster, both the iron atoms are trivalent and coupled anti-ferromagnetically, forming an $S = 0$ ground state. Therefore, the oxidized [2Fe-2S] cluster is EPR silent. In the samples reduced by sodium dithionite, EPR signals arising from the $S = 1/2$ ground state formed by anti-ferromagnetically coupled Fe^{3+} ($S = 2$) and Fe^{2+} ($S = 3/2$) were observed. EPR spectra of the ^{14}N- and ^{15}N-Rieske clusters [2Fe-2S] showed identical rhombic signals. The principal values of the g-tensor were 1.81, 1.90, and 2.03 for g_x, g_y, and g_z, respectively, which are similar to those of the reduced cluster [2Fe-2S] of other photosynthetic organisms. Principal g-values of 1.76, 1.90, and 2.03 were reported in an isolated cytochrome bc_1 complex from *R. sphaeroides*[22, 23]. Earlier work reported g_x of 1.815 and g_y of 1.90.[24] Although no g_z value has been reported, the other g-values, g_x and g_y, obtained in this work are identical to the previous report[24].

ESEEM and HYSCORE experiments were performed under the field corresponding to each principal value of the g-tensor. At the magnetic field corresponding to the g_x and g_z positions, the direction of the magnetic field is only limited to the x- and z-axes, respectively, and thus, oriented and selected 'single crystal-like' spectra were observed.

3.2. Three-pulse ESEEM

Fig. 5 shows the three-pulse ESEEM spectra of the reduced Rieske [2Fe-2S] center observed at the position of g_i ($i=x, y, z$). In all ESEEM spectra, the peaks arising from double quantum transitions were detected in the region of 5–9 MHz. These strongly coupled nitrogen signals were assigned as the nitrogen of the histidine ligands[20, 25]. Two peaks were detected at g_y and g_z, arising from different histidine molecules. In the g_x spectra, the two signals were not completely separated, indicating that two nitrogen atoms have similar hyperfine couplings. In all the magnetic fields, three strong peaks were observed in the region of 0–5 MHz. However, the hyperfine and quadrupole couplings of ^{14}N cannot be determined from the three-pulse ESEEM spectra, because of the overlapping of multiple ^{14}N signals. Higher resolution HYSCORE is required to determine the magnetic parameters of multiple ^{14}N atoms.

3.3 HYSCORE observed at g_z

Fig. 6 shows the HYSCORE spectra of the reduced [2Fe-2S] cluster in the ^{14}N and ^{15}N Rieske proteins observed at g_z. The strongest peaks were assigned to correlations of double-double (dd) quantum transitions of ^{14}N that were strongly coupled to the [2Fe-2S] cluster, denoted as 1_{dd}, with the coordinates of (-3.54, 7.08)/(-7.08, 3.54) MHz in the (- +) quadrant of the ^{14}N-HYSCORE spectra. In addition, there are strong peaks, denoted by 2_{dd}, with the coordinates of (-8.30, 4.52)/(-4.52, 8.30) MHz, which are related to the double-double quantum transitions arising from another ^{14}N that is strongly coupled to the [2Fe-2S] cluster. The other peaks are observed at the positions of (-2.69, 7.20) /(-7.20, 2.69) MHz, (-8.30, 3.42)/(-3.42, 8.30) MHz, and (-8.30, 2.93)/(-2.93, 8.30) MHz, denoted by 1_{ds}, 2_{ds}, and $2'_{ds}$, respectively. The peaks were assigned to the double-single transitions of nitrogen 1 and nitrogen 2, respectively. The 2_{ds} and 2_{ds}' peaks were resolved under different measurement conditions (Fig. S1). These correlation peaks give nuclear frequencies: N_{1z+} (3.54, 2.69, and 0.85) MHz with quadrupole splitting $3|Q_z|$ =1.84 MHz. We assumed that quadrupole interaction contributes to both sq frequencies. From Eq.(1) and (2), a second nuclear frequencies set was determined as (7.08, 2.65, and 4.49) MHz for nitrogen 1. Based on the *dd*-peak frequencies, the hyperfine component A_z is 4.67 MHz using formula (9). For Nitrogen 2, the nuclear frequencies are obtained as (8.30, 5.31, 2.99) and (4.52, 3.42, 1.10) MHz for 2, and (8.30, 4.82, 3.48) and (4.52, 2.93, 1.59) MHz for 2', respectively. $2ds$ and $2'ds$ are also belonging to the same double quantum transition; however, they are not arising from the same nuclear frequencies (see discussions below). A_z for nitrogen 2 is obtained as 5.84 MHz for both 2 and 2'. The peaks S1 and S2 are the overlapped sq-sq of nitrogen 1 and 2. Furthermore, in the region of (0–5, 0–5) MHz in the ^{14}N-HYSCORE spectrum, there are overlapping signals of nitrogen 1, nitrogen 2, and other nitrogen signals.

In contrast to the ^{14}N HYSCORE spectrum, only two peaks are detected in the (– +) quadrant of the ^{15}N HYSCORE spectrum. Nuclear frequencies of ^{15}N determined from the peak positions are (-2.08, 4.78)/(-4.78, 2.08) MHz and (-2.93, 5.73)/(-5.73, 2.93)MHz for nitrogen 1 and 2, respectively. One ^{15}N interacting with an electron spin (S = 1/2) induces only two correlation peaks, and thus, the other peaks in the (+ +) quadrant are arising from the other ^{15}N, namely nitrogen 3 and 4. For ^{15}N, the nuclear frequencies of nitrogen 3 and 4 are (1.71, 1.22)/(1.22, 1.71) and (2.08, 0.85)/(0.85, 2.08) MHz, respectively. The

hyperfine constants for nitrogen 3 and 4 were determined as 0.49 and 1.22 MHz, respectively.

3.4 HYSCORE measured at g_x

Fig. 7 shows the HYSCORE spectra observed under the magnetic field at g_x. Correlation peaks of dq-dq transitions were detected at (-6.96, 2.93)/(-2.93, 6.96) and (-8.30, 4.03)/(-4.03, 8.30) MHz for 1_{dd} and 2_{dd}, respectively in the (– +) quadrant of the ^{14}N-HYSCORE spectrum. A_x was calculated as 4.34 and 5.67 MHz for nitrogen 1 and 2, respectively. Correlation peaks were detected at (-6.95, 1.34)/(-1.34, 6.95) and (-8.30, 2.69)/(-2.69, 8.30) MHz. Using the first order expressions, nuclear frequencies were calculated as (6.96, 3.61, 3.36) MHz and (2.93, 1.59, 1.34) MHz for nitrogen 1, and (8.30, 4.83, 3.48) MHz and (4.03, 2.69, 1.34) MHz for nitrogen 2. Quadrupole couplings, $3|Q_x|$, were calculated as 0.25 MHz for nitrogen 1 and 1.35 MHz for nitrogen 2. At the field corresponding to g_x, weak intensity signals were detected in the (+ +) quadrant of the ^{14}N-HYSCORE spectrum. In contrast, in the ^{15}N-HYSCORE spectrum (Fig. 7 below), clear correlation peaks arising from at least two nitrogen atoms (nitrogen 3 and 4) were detected at the peak positions (1.83, 1.49)/(1.49, 1.83) MHz for nitrogen 3 and (2.32, 0.98)/(0.98, 2.32) for nitrogen 4, respectively. This indicates that the hyperfine couplings of nitrogen 3 and 4 in the field direction corresponding to the g_x axis are 0.34 MHz and 1.34 MHz, respectively.

3.5 HYSCORE measured at g_y

At the field of the g_y position, molecular orientations are directed towards other directions in addition to the principal g_y axis. Therefore, the HYSCORE spectra at g_y were expected to be powder-like patterns. Fig. 8 (top) shows the ^{14}N-HYSCORE spectrum measured at g_y. The strongest peaks in the (– +) quadrant arise from the correlations of two double quantum transitions of ^{14}N, which are strongly coupled to the iron-sulfur cluster. Peak positions of dq-dq transitions were observed at (-6.47, 2.69)/(-2.69, 6.47) MHz and (-7.45, 3.42)/(-3.42, 7.45) MHz for nitrogen 1 and 2, respectively. From two frequencies of the dq-dq transitions, the hyperfine couplings were obtained as 3.97 MHz and 4.94 MHz for nitrogen 1 and 2, respectively. The correlated single quantum transitions (sq) were also detected, denoted by S1 and S2, at (-3.78, 1.71)/(-1.71, 3.78) MHz and (-2.89, 0.98)/(-0.98, 2.89) MHz, respectively. The 1_{ds} $1'_{ds}$, and

2_{ds} peaks correlate with the double quantum and single quantum transitions (dq-sq) at the coordinates (-6.47, 0.85)/(-0.85, 6.47) MHz, (-6.47, 1.71)/(-1.71. 6.47) MHz and (-7.45, 2.81)/(-2.81, 7.45) MHz, respectively. From these peak positions, the nitrogen nuclear frequencies and the magnetic parameter were calculated based on the method described by eqs (1)-(3): v_{1y+} = (6.47, 3.73, 2.74) MHz, v_{1y-}= (2.69, 1.84, 0.85) MHz, $3|Q_y|$ = 0.99 MHz, A_{1y} = 4.23 MHz and 4.93 MHz and A_y = 3.97 MHz. Fig. 8 (bottom) shows the ^{15}N-HYSCORE spectrum measured at g_y. In the (- +) quadrant, the strongly coupled correlation peaks were observed at (-4.40, 1.34)/(-1.34, 4.40) MHz and (-5.01, 1.95)/(-1.95, 5.01) MHz for nitrogen 1 and 2, respectively. The hyperfine constants (^{15}N) were calculated as 5.74 MHz and 6.96 MHz for nitrogen 1 and 2, respectively. Weakly coupled nitrogen signals were observed in the (+ +) quadrant. Nitrogen 3 signal was not separated in the g_y because of the significantly weak hyperfine coupling ~ 0 MHz. Resolution of the data points of the ^{15}N-HYSCORE spectra is ~0.12 MHz, therefore the magnitudes of the hyperfine coupling is less than 0.24 MHz. Nuclear frequencies for nitrogen 4 were (2.20, 0.98)/(0.98, 2.20) MHz, which led to a hyperfine constant of 1.22 MHz. All the magnetic parameters determined from the HYSCORE spectra are summarized in Table 1 for strongly coupled nitrogen 1 and 2, and in Table 2 for weakly coupled nitrogen 3 and 4. Figs. S2-S4 shows the simulated HYSCORE spectra.

4. Discussions

4.1 Comparison of the stimulated ESEEM spectra with that of the photosynthetic Rieske [2Fe-2S] cluster

Britt et al. have reported the stimulated ESEEM spectra of spinach Rieske protein[25] observed only at the maximum of the ESE signal, which corresponds to the ESEEM spectra observed at g_y (Fig. 5). In spinach Rieske protein, the strong ESEEM peak was detected at around 4 MHz. Similar peaks were detected in *Rhodospirillum sphaeroides* and *Rhodobacter sphaeroides* R-26. These peaks are different from those observed at g_y in the present work (Fig. 5). Alternatively, the stimulated ESEEM spectrum measured at g_z of *C. tepidum* were similar to those of spinach and purple bacteria observed at g_z. The difference between *C. tepidum* and other photosynthetic organisms is attributed to the weakly coupled nitrogen atoms. The possible weakly coupled nitrogen

is peptide nitrogen that has a hydrogen bond with the [2Fe-2S] cluster or Nε of the direct ligand, histidine. Samoilova et al. have reported the differences of the stimulated ESEEM peaks are caused by the different Q_O-site occupants in Rieske center, where the peaks in g_z and g_x are more sensitive than that in g_y peaks[26]. Therefore, the differences among photosynthetic organisms may be ascribed to the differences of the peptide nitrogen.

4.2 Environment of histidine

HYSCORE results showed two different nitrogen signals with large hyperfine couplings, labeled nitrogen 1 and nitrogen 2. These signals arise from the nitrogen in histidine directly ligated to Fe^{2+}. The hyperfine couplings and quadrupole constants for g_x and g_y are similar with both the high-potential type and low-potential type[17] iron-sulfur clusters, which indicate that the Rieske [2Fe-2S] cluster of *C. tepidum* has two histidine ligands and the dihedral angles between histidine and 2Fe-2S plane are similar in structure between high and low potential type Rieske proteins.

In the well-resolved ^{14}N-HYSCORE spectrum observed at g_z (Fig. S1 top), the dq-sq transition correlation peaks were separated as 2_{ds} and $2'_{ds}$. The nuclear frequencies of the single quantum transitions were 3.42 MHz for 2_{ds} and 2.93 MHz for 2_{ds}'. The sum of these frequencies is 6.35 MHz, which is inconsistent with (also see Fig. 3):

$$v_{1sq\pm} + v_{2sq\pm} = v_{dq\pm} \qquad (12)$$

The double quantum transition of 8.30 and 4.52 MHz is arising from the nitrogen 2 of histidine directly ligated to Fe. The two single quantum transitions have almost the same hyperfine constants, but different quadrupole constants. Usually, the anisotropy of single quantum transitions is larger than double quantum transitions. Therefore, one can suggest that 2_{ds} and $2'_{ds}$ are just two points of the same ds ridge of low intensity. The signals influenced by τ-suppression and appeared randomly in the spectrum which is actually the sum of different spectra. Estimations of the quadrupole coupling remain ambiguities. Therefore, the determined quadrupole couplings (Q_x, Q_y, Q_z) are not traceless. (See supporting information for more discussions for the quadrupole couplings of the N_1 and N_2.)

The weakly coupled nitrogen 3 signals were assigned as the remote nitrogen (Nε) of the histidine

coordinating His126 or His145. Hyperfine couplings of $^{15}N\varepsilon$ were 0.35, ~0, and 0.48 MHz for g_x, g_y, and g_z, respectively. Average of the hyperfine coupling of the three directions are 0.27-0.35 MHz. In the cytochrome bc_1 complex of *R. sphaeroides*, similar hyperfine couplings of 0.3 – 0.4 MHz were obtained and assigned as the remote $N\varepsilon$[22]; however, the obtained anisotropy was very small (~0.1 MHz). In contrast, the anisotropy of *C. tepidum* is larger than 0.1 MHz (Table S2). The isotropic and anisotropic hyperfine couplings depend on the spin density on the 2s and 2p orbitals, respectively. The differences indicate that electron spin density on the 2p orbital increased. The remote N of the histidine ligand is the quinol binding site and quinone-His-Fe would be a main electron transfer pathway. The different electronic structure of the histidine would imply a substate, which influence the electron transfer rate from quinol to the iron-sulfur cluster. It is notable that [2Fe-2S] cluster has two histidine ligands and both remote $N\varepsilon$ might contribute to the N3 signals. However, the obtained anisotropy of hyperfine coupling is relatively larger. Therefore, the possibility is unlikely that two equivalent $N\varepsilon$ contributes. There are some possibilities: (1) the hyperfine coupling of one $N\varepsilon$ is relatively small; (2) observed anisotropy is effectively large because of overlapping of two remote nitrogen signals. In both case, it is difficult to distinguish two nitrogen signals. Use of single crystal would help to clarify them in the future.

4.3 Protein backbone

Hyperfine couplings of 1.2 – 1.4 MHz were detected in the ^{15}N-HYSCORE spectra and are denoted as nitrogen 4. Similar HYSCORE spectra were previously acquired[27, 28]. In the stimulated ESEEM spectra of *C. tepidum*, multiple weakly coupled nitrogen signals were observed in the region of 0 – 5 MHz. In the Rieske cluster [2Fe-2S], the unpaired electron spin is distributed not only at the Fe sites, but also in peptide nitrogen via the sulfur and hydrogen bond. The weakly coupled nitrogen signal indicates that there is at least one peptide nitrogen atom connected to the [2Fe-2S] center via hydrogen bonding. The H-bond structure is essential for regulating the midpoint potentials[12-15].

Dikanov et al.[22] showed that the peptide nitrogen in the cytochrome *bc* complex of purple bacteria has a small anisotropy associated with its hyperfine coupling. The hyperfine couplings of peptide nitrogen were in the range of 1.1 - 1.2 MHz at several *g*-values. In the ferredoxin of red marine algae *Porphira umbilicalis*, 1.08 MHz of ^{14}N (1.51 MHz of ^{15}N) hyperfine coupling of peptide nitrogen was detected[29]. The small field dependence of the hyperfine couplings indicates that isotropic hyperfine interactions occur dominantly with nitrogen 4. These values are similar to the *C. tepidum*, but the isotropic hyperfine couplings are significantly different. The larger isotropic hyperfine couplings indicate that spin density is more distributed at the peptide nitrogen. The spin density orbital reflects the modification of the H-bond structure surrounding sulfur. The result suggests that the hydrogen bond length and/or angle are different. The H-bond structure is different between *C. tepidum* and purple bacteria and possibly modifies the midpoint potentials. Additionally, Dikanov et al.[22] assigned the detected peptide nitrogen signal to Leu132, which is a conserved amino acid residue during the course of evolution. Leu132 in *R. sphaeroides* is Leu110 in spinach (See Fig. 1 and Fig. 2). However, the crystal structure of *C. tepidum* has not been reported yet. Other amino acid residues are also possibly contributed to nitrogen 4 signal via the hydrogen bond.

5. Conclusion

In this paper, an ESEEM study of the Rieske protein of *C. tepidum* was reported. The protein environments surrounding the [2Fe-2S] cluster were characterized by ^{14}N- and ^{15}N-HYSCORE spectroscopy. Our results for green sulfur bacteria were compared with previous reports in other photosynthetic organisms. The results show that the electronic and hydrogen bond structures are slightly different between green sulfur bacteria and other photosynthetic organisms, although their main structures are similar. These differences would cause modification of the midpoint potentials of the iron-sulfur cluster in order to adjust to an oxygen-rich environment during the course of evolution.

The complete structure of the H-bonding is still unclear because of the lack of structural information of the Rieske protein in *C. tepidum*. X-ray crystal structure analysis combined with HYSCORE spectroscopy using single crystals and site-specific isotope labeling would allow the hydrogen bond structure surrounding the [2Fe-2S] cluster to be determined.

AUTHOR INFORMATION

Corresponding Author

To whom correspondence should be addressed: Graduate school of Science, Nagoya University, Furo-cho, Chikusa, Nagoya, 464-8602, Japan. Tel: +81-52-789-2883; Fax: +81-52-789-2883; E-mail: mino@bio.phys.nagoya-u.ac.jp.

Present Addresses

Risa Mutoh, Department of Applied Physics, Faculty of Science, Fukuoka University, 8-19-1, Nanakuma, Jonan-ku, Fukuoka, 814-0180, Japan

Author Contributions

H.N., R.M., H.O., G.K., and H.M. designed this study and wrote this paper. H.N., N.T., and H.M. measured the EPR and ESEEM spectra, and analyzed the experimental results. H.K. and R.M. prepared samples of the Rieske protein from *C. tepidum*.

ACKNOWLEDGMENT

SUPPORTING INFORMATION

Highly resolved ^{14}N-HYSCORE spectra, discussion of detailed quadrupole couplings, simulations of HYSCORE using magnetic parameters derived from experiments, simulations of HYSCORE with the principal values of hyperfine and quadrupole tensors and Euler angle rotations.

FIGURE CAPTION

Fig. 1 Alignment of amino acid sequences of spinach (Uniprot ID: P08980), *R. sphaeroides* (Q02762) and *C. tepidum* (Q9F722). Three amino acid sequences were aligned using Clustal X version 2.1.[30]

Fig. 2 (A) X-ray crystal structures of Rieske proteins isolated from spinach (PDB ID: 1RFS). Amino acid residues within 6 Å from the iron-sulfur center are shown.

S130 is substituted by alanine in green sulfur *C. tepidum*. (B) The Rieske protein structure in spinach (in multi-color) and purple bacteria *R. sphaeroides* (PDB: 2QJY) (in light blue). The dashed line shows the direct ligation of Fe (black) and the hydrogen bond (red). Color schemes: C, gray; O, red; N, blue; S, yellow; Fe, brown.

Fig. 3 Energy diagram of nitrogen nuclei interacting with an electron spin of $S = 1/2$. ^{14}N ($I = 1$) has three sublevels and ^{15}N ($I = 1/2$) has two sublevels for each electron spin manifold ($m_s = \pm 1/2$). The transitions between adjacent nuclear sublevels with frequencies, ν_{sq}, are single quantum transitions. The transitions between extreme sublevels with frequencies, ν_{dq}, are double-quantum transitions.

Fig. 4 CW-EPR spectra of the [2Fe-2S] cluster of the ^{14}N- and ^{15}N-Rieske proteins. Principal values of the g-tensor are defined as $(g_x, g_y, g_z) = (1.81, 1.90,$ and $2.03)$. The measurement conditions were as follows: the microwave frequency was 9.626 GHz for ^{15}N and 9.659 GHz for ^{14}N, and the microwave power, modulation amplitude, time constant, conversion time, and temperature were 0.4 mW, 0.6 mT, 40.96 ms, 40.96 ms, and 12 K, respectively.

Fig. 5 Three-pulse ^{14}N-ESEEM spectra obtained under the field corresponding to the three principal g-values (g_x, g_y, g_z). Static magnetic fields were at 374, 357 and 337 mT for g_x, g_y, g_z, respectively. The delay time between first and second pulse $\tau = 160, 200,$ and 240 ns were used to eliminate blind spots.

Fig. 6 The frequency-domain contour plots of the HYSCORE spectra obtained under the magnetic field corresponding to $g_z = 2.03$. Panels (A and B) are ^{14}N-HYSCORE and panels (C and D) are ^{15}N-HYSCORE spectra. Spectra (A) and (C) are the stacked plots of (B) and (D), respectively. Static magnetic field was 341 (^{14}N) and 338 mT (^{15}N). The ^{14}N-HYSCORE spectra were acquired at $\tau = 188, 200,$ and 216 ns.

Fig. 7 The frequency-domain contour plots of the HYSCORE spectra measured under the magnetic field corresponding to g_x. Panels (A and B) are ^{14}N-HYSCORE and panels (C and D) are ^{15}N-HYSCORE spectra. Spectra (A) and (C) are the stacked plots of (B) and (D), respectively. Static magnetic field was 380 (^{14}N) and 377 mT(^{15}N) The measurement conditions apart from the magnetic field were the same as those described in the Fig. 6 caption.

Fig. 8 The frequency domain contour plots of the HYSCORE spectra obtained under the magnetic field corresponding to g_y. Panels (A and B) are ^{14}N-HYSCORE and panels (C and D) are ^{15}N-HYSCORE

spectra. Spectra (A) and (C) are the stacked plots of (B) and (D), respectively. Static magnetic field was 363 (^{14}N) and 361 mT (^{15}N). The measurement conditions apart from the magnetic field were the same as those described in the Fig. 6 caption.

Table 1 Nuclear frequencies and magnetic parameters for the strongly coupled nitrogen signals observed with ^{14}N-HYSCORE spectroscopy measured under the fields corresponding to g_x, g_y, and g_z. The units is in megahertz (MHz). The numbers assigned to the nitrogens correspond to the marked numbers in the HYSCORE spectra. The frequencies in parentheses belong to the same set of nuclear sublevel transitions.

Table 2 Nuclear frequencies and magnetic parameters for the weakly coupled nitrogen signals determined from ^{15}N-HYSCORE spectroscopy measured under the fields corresponding g_x, g_y, and g_z. The units are in MHz. The numbers assigned to the nitrogens correspond to the marked numbers in the HYSCORE spectra. The hyperfine values in parentheses show the calculated ^{14}N hyperfine couplings.

REFERENCES

(1) Crofts, A. R., The cytochrome bc₁ complex: Function in the context of structure. *Annu Rev Physiol* **2004,** *66*, 689-733.

(2) Kramer, D. M.; Nitschke, W.; Cooley, J. W., The cytochrome bc₁ and related bc complexes: the Rieske/cytochrome b complex as the functional core of a central electron/proton transfer complex. In *The purple phototrophic bacteria*, Springer: 2009; pp 451-473.

(3) Schütz, M.; Zirngibl, S.; le Coutre, J.; Büttner, M.; Xie, D.-L.; Nelson, N.; Deutzmann, R.; Hauska, G., A transcription unit for the Rieske FeS-protein and cytochrome b in Chlorobium limicola. *Photosynth Res* **1994,** *39*, 163-174.

(4) Tsukatani, Y.; Azai, C.; Kondo, T.; Itoh, S.; Oh-oka, H., Parallel electron donation pathways to cytochrome c_z in the type I homodimeric photosynthetic reaction center complex of Chlorobium tepidum. *Biochim Biophys Acta* **2008,** *1777*, 1211-1217.

(5) Xiong, J.; Inoue, K.; Bauer, C. E., Tracking molecular evolution of photosynthesis by characterization of a major photosynthesis gene cluster from Heliobacillus mobilis. *Proc Nat Acad Sci* **1998,** *95*, 14851-14856.

(6) Schütz, M., *et al.*, Early evolution of cytochrome bc complexes. *J Mol Biol* **2000,** *300*, 663-675.

(7) Zu, Y. B.; Couture, M. M. J.; Kolling, D. R. J.; Crofts, A. R.; Eltis, L. D.; Fee, J. A.; Hirst, J., Reduction potentials of Rieske clusters: Importance of the coupling between oxidation state and histidine protonation state. *Biochemistry* **2003,** *42*, 12400-12408.

(8) Liu, J.; Chakraborty, S.; Hosseinzadeh, P.; Yu, Y.; Tian, S.; Petrik, I.; Bhagi, A.; Lu, Y., Metalloproteins containing cytochrome, iron-sulfur, or copper redox centers. *Chem Rev* **2014,** *114*, 4366-4469.

(9) Link, T. A., The structures of Rieske and Rieske-type proteins. *Adv Inorg Chem* **1999,** *47*, 83-157.

(10) Ullmann, G. M.; Noodleman, L.; Case, D. A., Density functional calculation of pK_a values and redox potentials in the bovine Rieske iron-sulfur protein. *J Biol Inorg Chem* **2002,** *7*, 632-639.

(11) Esser, L.; Elberry, M.; Zhou, F.; Yu, C. A.; Yu, L.; Xia, D., Inhibitor-complexed structures of the cytochrome bc₁ from the photosynthetic bacterium Rhodobacter sphaeroides. *J Biol Chem* **2008,** *283*, 2846-2857.

(12) Denke, E.; Merbitz-Zahradnik, T.; Hatzfeld, O. M.; Snyder, C. H.; Link, T. A.; Trumpower, B. L., Alteration of the midpoint potential and catalytic activity of the rieske iron-sulfur protein by changes of amino acids forming hydrogen bonds to the iron-sulfur cluster. *J Biol Chem* **1998,** *273*, 9085-9093.

(13) Guergova-Kuras, M.; Kuras, R.; Ugulava, N.; Hadad, I.; Crofts, A. R., Specific mutagenesis of the Rieske iron-sulfur protein in Rhodobacter sphaeroides shows that both the thermodynamic gradient and the pK of the oxidized form determine the rate of quinol oxidation by the bc₁ complex. *Biochemistry* **2000,** *39*, 7436-7444.

(14) Ashizawa, R.; Noguchi, T., Effects of hydrogen bonding interactions on the redox potential and molecular vibrations of plastoquinone as studied using density functional theory calculations. *Phys Chem Chem Phys* **2014,** *16*, 11864-11876.

(15) Schroter, T.; Hatzfeld, O. M.; Gemeinhardt, S.; Korn, M.; Friedrich, T.; Ludwig, B.; Link, T. A., Mutational analysis of residues forming hydrogen bonds in the Rieske [2Fe-2S] cluster of the cytochrome bc₁ complex in Paracoccus denitrificans. *Eur J Biochem* **1998,** *255*, 100-106.

(16) Carrell, C. J.; Zhang, H. M.; Cramer, W. A.; Smith, J. L., Biological identity and diversity in photosynthesis and respiration: structure of the lumen-side domain of the chloroplast Rieske protein. *Structure* **1997,** *5*, 1613-1625.

(17) Dikanov, S. A.; Shubin, A. A.; Kounosu, A.; Iwasaki, T.; Samoilova, R. I., A comparative, two-dimensional ^{14}N ESEEM characterization of reduced [2Fe-2S] clusters in hyperthermophilic archaeal high- and low-potential Rieske-type proteins. *J Biol Inorg Chem* **2004,** *9*, 753-767.

(18) Takahashi, Y.; Nakamura, M., Functional assignment of the ORF2-iscS-iscU-iscA-hscB-hscA-fdx-oRF3 gene cluster involved in the assembly of Fe-S clusters in Escherichia coli. *J Biochem* **1999,** *126*, 917-926.

(19) Dikanov, S. A.; Xun, L. Y.; Karpiel, A. B.; Tyryshkin, A. M.; Bowman, M. K., Orientationally-selected two-dimensional ESEEM spectroscopy of the Rieske-type iron-sulfur cluster in 2,4,5-trichlorophenoxyacetate monooxygenase from Burkholderia cepacia AC1100. *J Am Chem Soc* **1996,** *118*, 8408-8416.

(20) Gurbiel, R. J.; Batie, C. J.; Sivaraja, M.; True, A. E.; Fee, J. A.; Hoffman, B. M.; Ballou, D. P., Electron nuclear double-resonance spectroscopy of ^{15}N-enriched phthalate dioxygenase from Pseudomonas-cepacia proves that 2 histidines are coordinated to the [2Fe-2S] Rieske-type clusters. *Biochemistry* **1989,** *28*, 4861-4871.

(21) Dikanov, S. A.; Tyryshkin, A. M.; Huttermann, J.; Bogumil, R.; Witzel, H., Characterization of histidine coordination in VO²⁺-substituted D-Xylose isomerase by orientationally-selected electron spin-echo envelope modulation spectroscopy. *J Am Chem Soc* **1995,** *117*, 4976-4986.

(22) Dikanov, S. A.; Kolling, D. R.; Endeward, B.; Samoilova, R. I.; Prisner, T. F.; Nair, S. K.; Crofts, A. R., Identification of hydrogen bonds to the Rieske cluster through the weakly coupled nitrogens detected by electron spin echo envelope modulation spectroscopy. *J Biol Chem* **2006,** *281*, 27416-27425.

(23) Andrews, K. M.; Crofts, A. R.; Gennis, R. B., Large-scale purification and characterization of a highly-active 4-subunit cytochrome *bc1* complex from *Rhodobacter sphaeroides*. *Biochemistry* **1990,** *29*, 2645-2651.

(24) Brugna, M.; Albouy, D.; Nitschke, W., Diversity of cytochrome bc complexes: Example of the Rieske protein in green sulfur bacteria. *J Bacteriol* **1998,** *180*, 3719-3723.

(25) Britt, R. D.; Sauer, K.; Klein, M. P.; Knaff, D. B.; Kriauciunas, A.; Yu, C. A.; Yu, L.; Malkin, R., Electron-spin echo envelope modulation spectroscopy supports the suggested coordination of

two histidine ligands to the Rieske Fe-S centers of the cytochrome b_6f Complex of spinach and the cytochrome bc_1 complexes of *Rhodospirillum rubrum, Rhodobacter sphaeroides* R-26, and bovine heart mitochondria. *Biochemistry* **1991,** *30,* 1892-1901.

(26) Samoilova, R. I.; Kolling, D.; Uzawa, T.; Iwasaki, T.; Crofts, A. R.; Dikanov, S. A., The interaction of the Rieske iron-sulfur protein with occupants of the Q_o-site of the bc_1 complex, probed by electron spin echo envelope modulation. *J Biol Chem* **2002,** *277,* 4605-4608.

(27) Iwasaki, T.; Kounosu, A.; Uzawa, T.; Samoilova, R. I.; Dikanov, S. A., Orientation-selected ^{15}N-HYSCORE detection of weakly coupled nitrogens around the archaeal Rieske [2Fe-2S] center. *J Am Chem Soc* **2004,** *126,* 13902-13903.

(28) Iwasaki, T.; Kounosu, A.; Samoilova, R. I.; Dikanov, S. A., ^{15}N HYSCORE characterization of the fully deprotonated, reduced form of the archaeal Rieske [2Fe-2S] center. *J Am Chem Soc* **2006,** *128,* 2170-2171.

(29) Dikanov, S. A.; Tyryshkin, A. M.; Felli, I.; Reijerse, E. J.; Huttermann, J., C-band ESEEM of strongly coupled peptide nitrogens in reduced Two-iron ferredoxin. *J Magn Reson Ser B* **1995,** *108,* 99-102.

(30) Larkin, M. A.*, et al.,* Clustal W and clustal X version 2.0. *Bioinformatics* **2007,** *23,* 2947-2948.

Figure 1

```
                  :.             *    :      **  . .:*                              .                       *   :: .
spinach      ATSIPADNVPDMQKRETLNLLLLGALSLPTGYMLLPYASFFVPPG------------GGAGTGGTIAKD    57
R.sphaeroides ---MSNAEDHAGTRRDFLYYATAGAGAVATGAAVWPLINQMNPSADVQALASIFVDVSSVEPGVQLTVK    66
C.tepidum    ---MAQTGNFKSPAR--MSSLGQGAAPASAGAVTGGKPREEGLKG-VDFERRGFLQKIVGGVGAVVAVS    63
```



```
              *    :       .        *          *    *                 :.   .:     *      : .:******:
spinach      ALGNDVIAAEWLKTHAPGDRTLTQGLKGDP---------TYLVVESDKTLATFG----INAVCTHLGCV   113
R.sphaeroides FLGKPIFIRRRTEADIELGRSVQLGQLVDTNARNANIDAGAEATDQNRTLDEAGEWLVMWGVCTHLGCV   135
C.tepidum    TLYPVVRYIVPPAKKIKIVNELAVGPASDVPNGTG--KIYQFNDDKVIVVNHGGSLTAVSAICTHLGCL   130
```



```
                   .         *****::*  .  *::   ** *   *    .. *                 :    .    .
spinach      VP--FNAAENKFICPCHGSQYNNQGRVVRGPAPLSLALAHCDVDDGKVVFVPWTETDFRTGEAPWWSA   179
R.sphaeroides PIGGVSGDFGGWFCPCHGSHYDSAGRIRKGPAPENLPIPLAKFID--------ETTIQLG-------   187
C.tepidum    VH--WDEAADMIACPCHGAKYTQDGKIISGPQPLPLKQYKVKIEDG-------KIVVSIA------   181
```
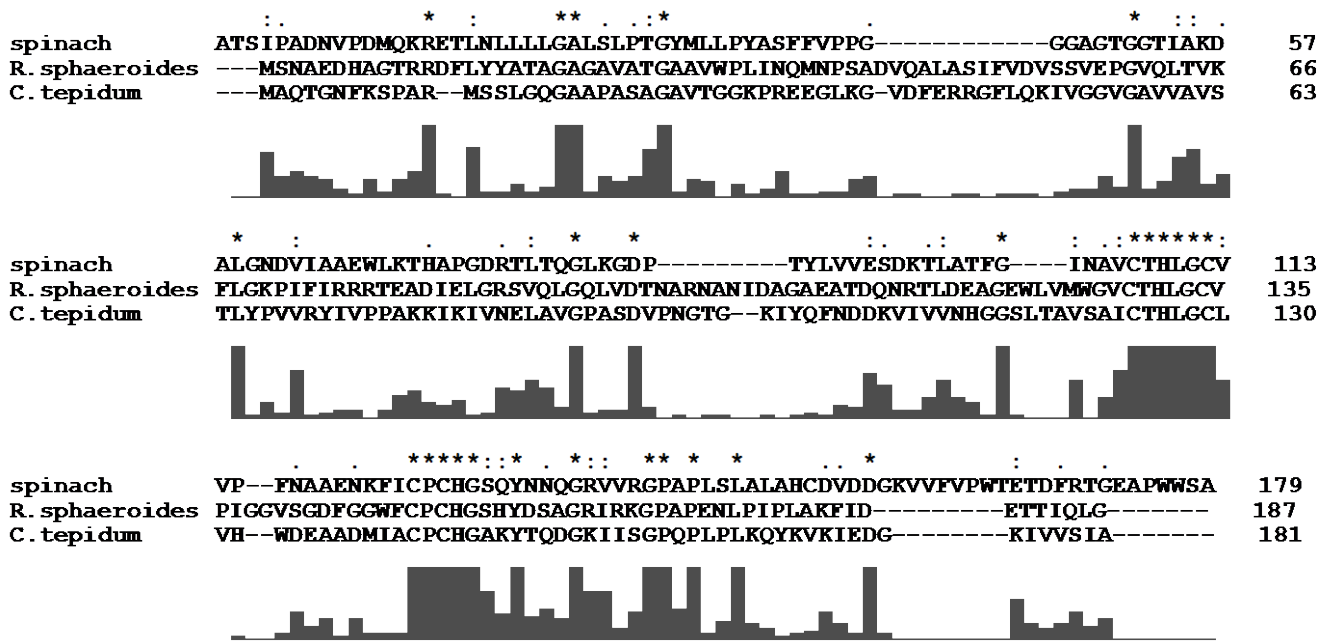

Figure2

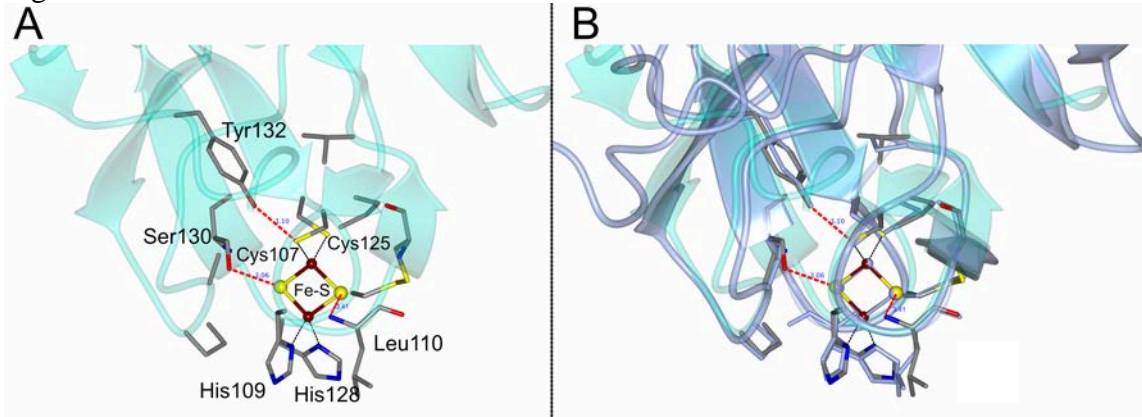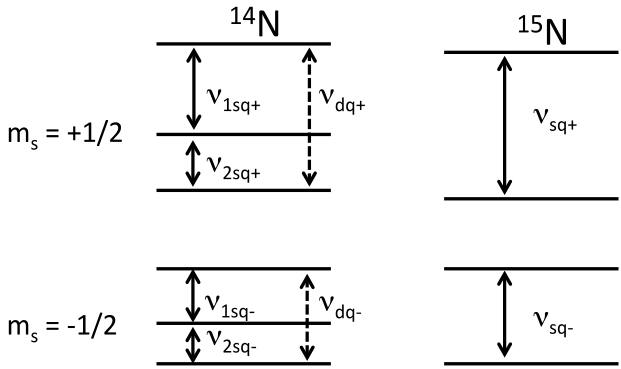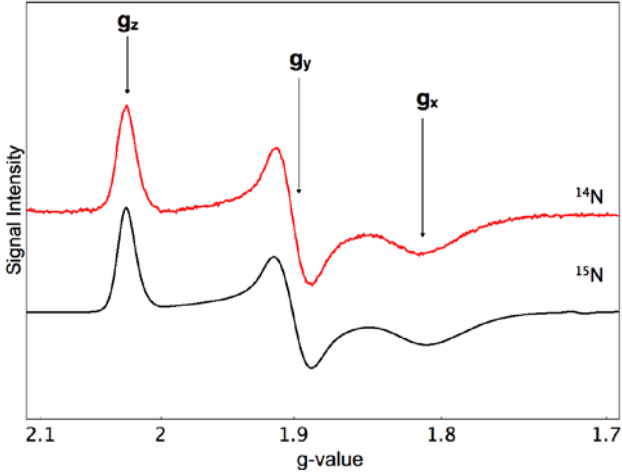Figure 3

Figure 4

Figure 5
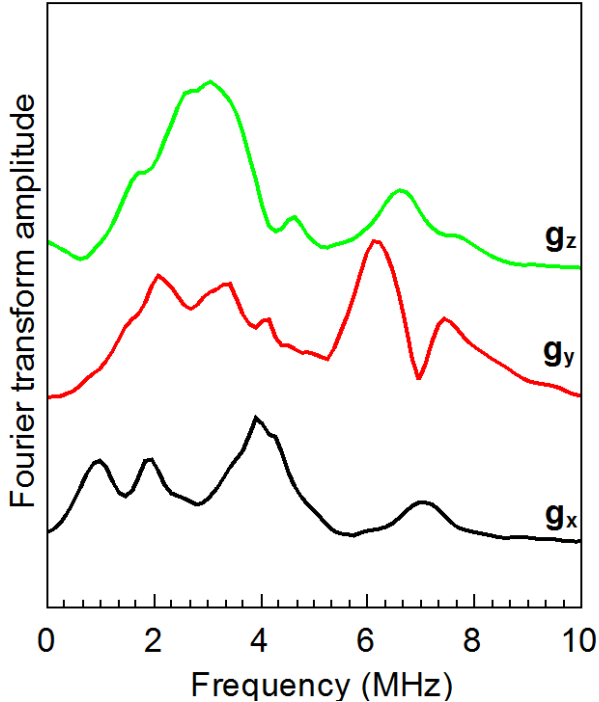
Figure 5
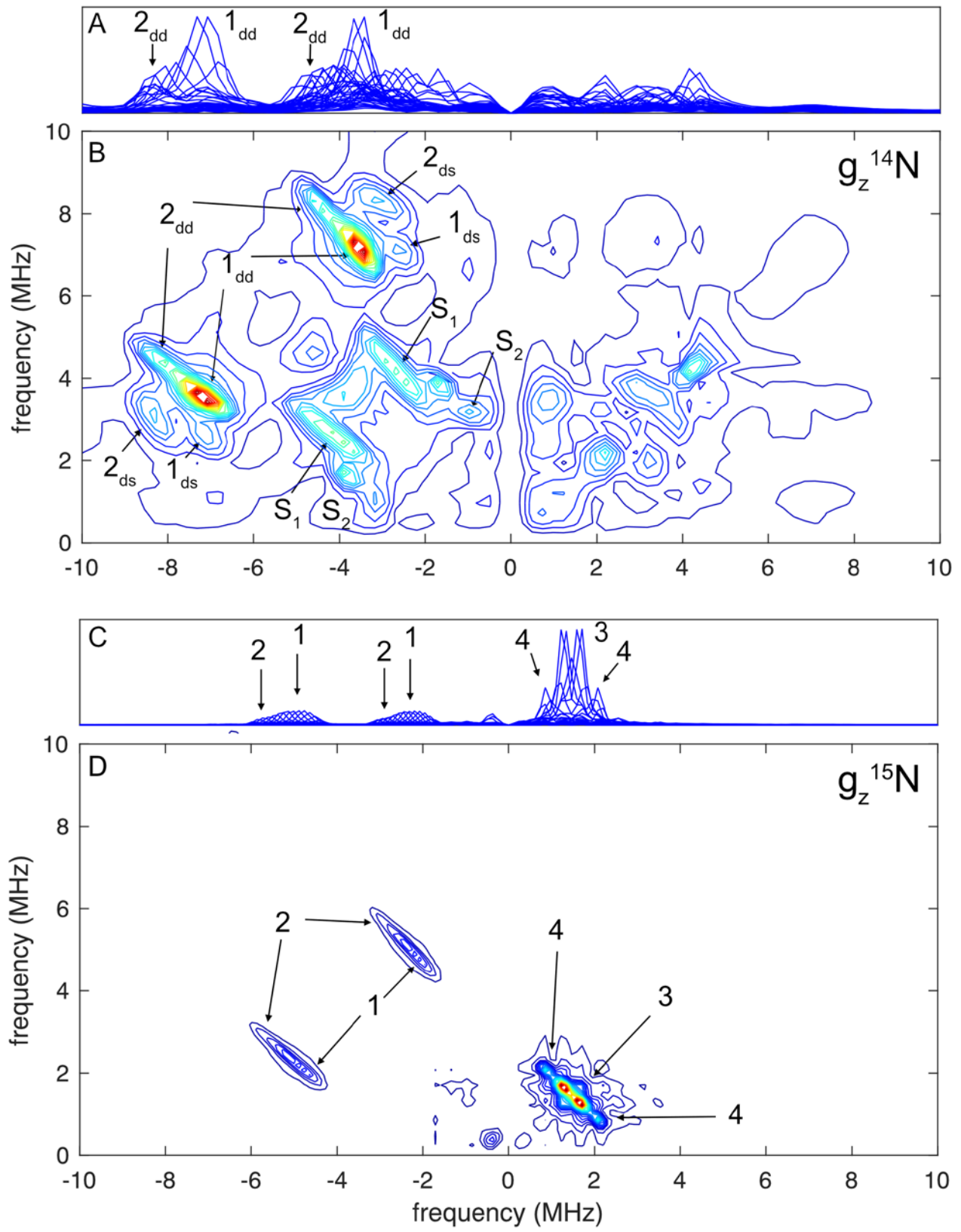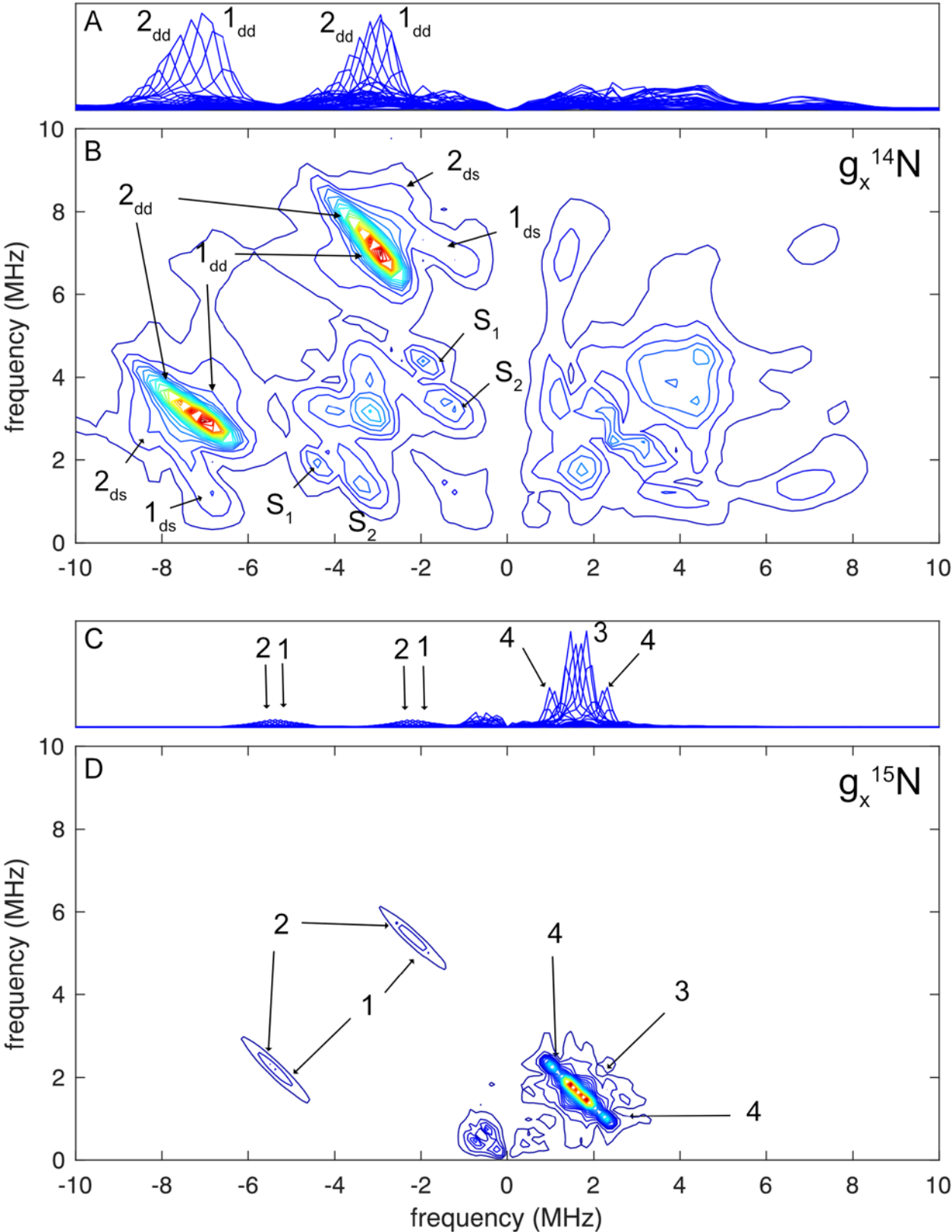
Figure 6

Figure 7

Figure 8

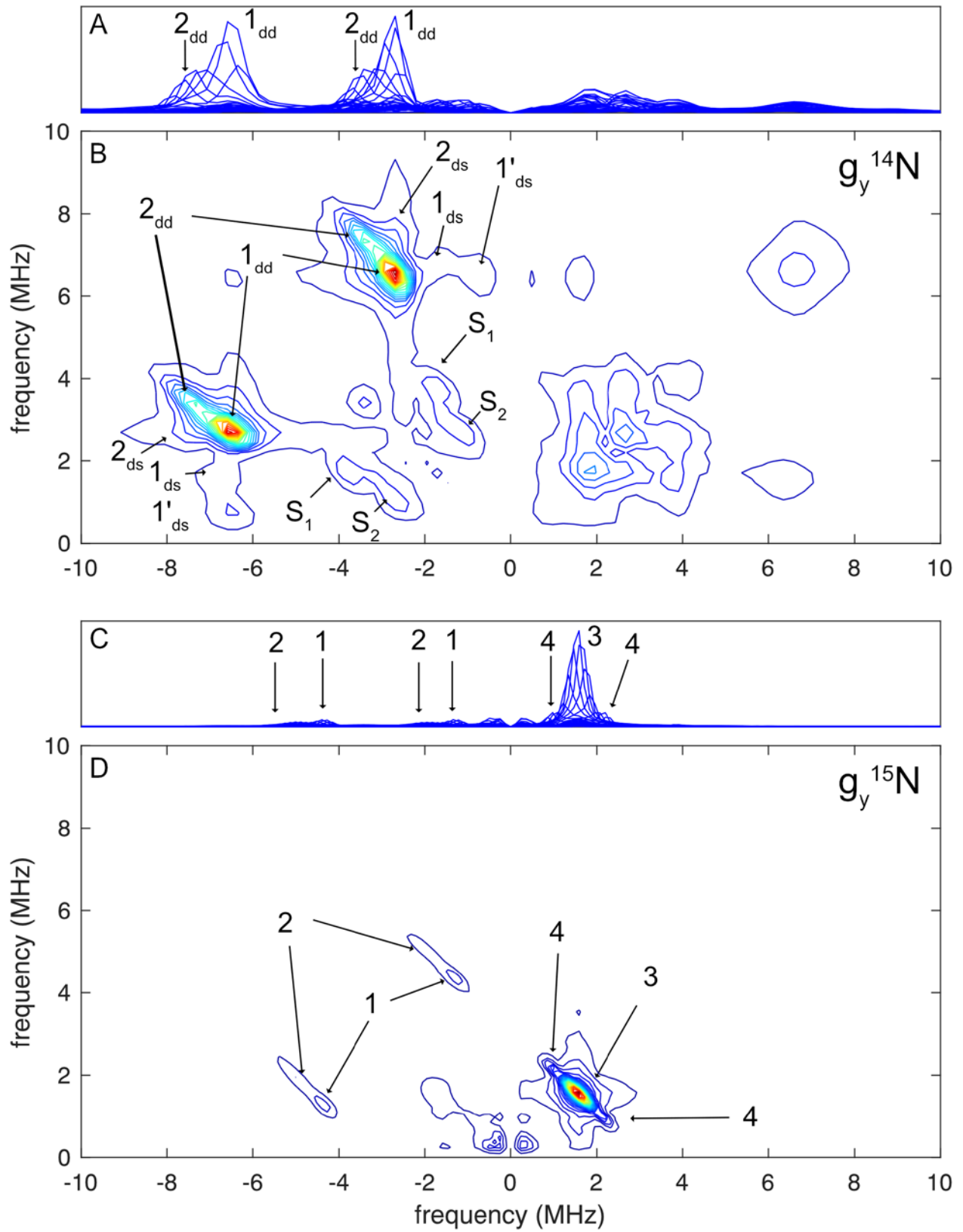Table 1

g-axis		N₁	N₂	N₁'	N₂'
	Sets of nuclear frequencies [a]	($\mathbf{6.96}$, 3.61, 3.36) ($\mathbf{2.93}$, 1.59, $\mathbf{1.34}$)	($\mathbf{8.30}$, 4.83, 3.48) ($\mathbf{4.03}$, $\mathbf{2.69}$, 1.34)		
	3 $|Q_x|$	0.25	1.35		
x	ν_I (^{14}N)	1.17	1.17		
	A_{1x} (^{14}N, ^{15}N)	4.62 (6.48) 5.27 (7.40)	5.96 (8.36) 6.37 (8.93)		
	A_x (^{14}N, ^{15}N)	4.34 (6.09)	5.67 (7.96)		
	Sets of nuclear frequencies [a]	($\mathbf{6.47}$, 3.73, 2.74) ($\mathbf{2.69}$, 1.84, $\mathbf{0.85}$)	($\mathbf{7.45}$, 2.63, 4.83) ($\mathbf{3.42}$, $\mathbf{2.81}$, 0.61)	($\mathbf{6.47}$, 3.60, 2.87) ($\mathbf{2.69}$, $\mathbf{1.71}$, 0.98)	
	3 $|Q_y|$	0.99	2.20	0.73	
y	ν_I (^{14}N)	1.12	1.12	1.12	
	A_{1y} (^{14}N, ^{15}N)	4.23 (5.93) 4.93 (6.92)	5.21 (7.31) 5.66 (7.94)	4.23, 4.93	
	A_y (^{14}N, ^{15}N)	3.97 (5.56)	4.94 (6.93)	3.97	
	Sets of nuclear frequencies [a]	($\mathbf{7.14}$, 2.65, 4.49) ($\mathbf{3.54}$, $\mathbf{2.69}$, 0.85)	($\mathbf{8.30}$, 5.31, 2.99) ($\mathbf{4.52}$, $\mathbf{3.42}$, 1.10)		($\mathbf{8.30}$, 4.82, 3.48) ($\mathbf{4.52}$, $\mathbf{2.93}$, 1.59)
	3 $|Q_z|$	1.84	2.32		1.34
z	ν_I(^{14}N)	1.05	1.05		1.05
	A_{1z} (^{14}N, ^{15}N)	4.64 (6.51) 5.04 (7.07)	6.20 (8.70) 6.62 (9.29)		6.2 (8.70) 6.62 (9.29)
	A_z (^{14}N, ^{15}N)	4.68 (6.56)	5.84 (8.19)		5.84

The spectral resolution of the HYSCORE spectroscopy is 0.1-0.2 MHz.

a) The bold values are directly obtained from the HYSCORE peaks. The others are derived from eqs. (1)-(3) and (9) (see text).

b) Hyperfine constants of ^{15}N were scaled by equation (11). N₁' and N₂' are corresponded to the same double quantum frequencies of N₁ and N₂, but with the other combinations of single quantum frequencies.

Table 2

g-axis		N_3	N_4
x	Nuclear frequencies	**1.83**, **1.49**	**2.32**, **0.98**
	hyperfine coupling: ^{15}N (^{14}N)	0.35 (0.25)	1.34 (0.95)
y	Nuclear frequencies	**1.59**, **1.59**	**2.20**, **0.98**
	hyperfine coupling: ^{15}N (^{14}N)	<0.24 (<0.17)	1.22 (0.86)
z	Nuclear frequencies	1.71, 1.22	2.08, 0.85
	hyperfine coupling: ^{15}N (^{14}N)	0.49 (0.34)	1.22 (0.87)

TOC graphic